RSC Advances

PAPER

Check for updates

Nonlinear electrical characteristics of core-satellite CaCu$_3$Ti$_4$O$_{12}$@ZnO doped silicone rubber composites

Jun Wang,[ac] Xilin Wang, ID *[b] Youwei Yao,[c] Juyi Guo,[b] Xiaogang Ouyang ID [b] and Zhidong Jia[b]

The application of polymer composites with electric field dependent nonlinear conductive and dielectric characteristics for high voltage equipment is an effective method to control electric field stress and disperse space charges. In this study, core-satellite CaCu$_3$Ti$_4$O$_{12}$@ZnO fillers were synthesized and doped into silicone rubber composites, and compared to a mixture of CaCu$_3$Ti$_4$O$_{12}$ and ZnO with the same filler concentration. The composites exhibited both nonlinear conductive and nonlinear dielectric properties with nanoparticle fillers for the first time. Both the nonlinear conductive coefficient and dielectric coefficient increased with filler concentration. The classical current-path model was utilized to explain the nonlinear conductive properties, while the interface-barrier-layer-capacitor model and double-depletion-layer model were introduced to explain the nonlinear dielectric properties, which would broaden the thinking for the fabrication of nonlinear composites.

1. Introduction

A safe insulation property is one of the key characteristics in electric power systems. The higher the voltage is, the better the insulation needs to be. The transmission line voltage is increased to 1100 kV in China now. Unexpected local enhancements of electric field on high voltage devices often appear in a complex electric environment, which would threaten the safety and stability of the power system. Besides designs of the insulation structure, the use of field grading materials with nonlinear conductive or dielectric properties is an effective approach to solving these problems,[1,2] for the functional electrical parameters of such composites would adapt with the electric field automatically.

Fillers with outstanding nonlinear properties such as conductivity are often doped into composites to obtain nonlinearity, which has been widely researched. For nonlinear conductive property, fillers such as ZnO, SiC, silica and carbon black have been studied for decades and they aid in electric field grading.[2] For nonlinear dielectric property, many efforts have been made to employ inorganic non-metallic materials with high dielectric permittivity as functional fillers such as barium titanate, lead zirconate titanate and so on.[3–7] Although the

dielectric permittivity of these composites varies with the electric field, the nonlinear dielectric coefficient is relatively poor, which is not very satisfactory and makes them less attractive.

Zinc oxide (ZnO) is famous for its excellent nonlinear conductive properties and has been widely used to protect electrical devices against overvoltage in power systems.[8,9] The typical application is as a zinc oxide arrester. Recently, ZnO microparticles were fabricated and employed as fillers, and the composites exhibited both nonlinear conductive and dielectric properties.[10] However, the high volume fraction of microparticles in the silicone rubber composites may lead to the degradation of other performances, which needs to be improved.

Copper calcium titanate (CaCu$_3$Ti$_4$O$_{12}$) is a perovskite-like tetragonal oxide with a very large dielectric constant.[11–13] With its high permittivity, it has been reported that CaCu$_3$Ti$_4$O$_{12}$ has remarkably strong nonlinear conductive characteristics for an intrinsic electrostatic barrier at grain boundaries.[14] The nonlinear coefficient of CaCu$_3$Ti$_4$O$_{12}$ is even greater than that of ZnO.[15] It therefore has the potential to be used in field grading materials. However, there has been no study to make use of the nonlinear behavior of both ZnO and CaCu$_3$Ti$_4$O$_{12}$ in previous literature.

In this paper, ZnO and CaCu$_3$Ti$_4$O$_{12}$ nanoparticles were employed as fillers to tailor both the conductive and dielectric properties of composites. Considering Tanaka has built a multi-core model to explain the excellent electrical properties of nanocomposites,[16,17] core-satellite CaCu$_3$Ti$_4$O$_{12}$@ZnO nanoparticles were synthesized and doped into silicone rubber composites. The composites exhibited both nonlinear conductive and nonlinear dielectric properties with nanoparticle fillers for the first time, which would broaden the application of nonlinear composites.

[a]School of Materials Science and Engineering, Tsinghua University, Beijing 100084, P. R. China

[b]Engineering Laboratory of Power Equipment Reliability in Complicated Coastal Environment, Graduate School at Shenzhen, Tsinghua University, Shenzhen 518055, P. R. China. E-mail: wang.xilin@sz.tsinghua.edu.cn

[c]Advanced Materials Institute, Graduate School at Shenzhen, Tsinghua University, Shenzhen 518055, P. R. China

2. Experimental

2.1 Materials

Copper calcium titanate ($CaCu_3Ti_4O_{12}$, grain size $\approx$ 500 nm) was purchased from Shanghai Dianyang Industry Corp. and zinc oxide (ZnO, grain size $\approx$ 50 nm) was purchased from Nanjing Yaonano Corp. Zinc acetate ($Zn(Ac)_2$), sodium hydroxide (NaOH) and silane coupling agent KH-151 were obtained from Aladdin Reagent. 110 methyl vinyl silicone rubber (molecular weight 600 000, vinyl mass fraction 0.03%) and its vulcanizing agent were brought from Zhejiang Wynca Chemical Industrial Group Corp. Muscovite (IMERYS, US), aluminium hydroxide (AH-1, Aluminum Corporation of China Limited) and fumed silica (HL-200, Guangzhou GBS) were also used in this work.

2.2 Synthesis of core-satellite $CaCu_3Ti_4O_{12}$@ZnO

$Zn(Ac)_2$, NaOH and $CaCu_3Ti_4O_{12}$ nanoparticles were used for the synthesis of core-satellite $CaCu_3Ti_4O_{12}$@ZnO nanomaterials. The typical reaction between $Zn(Ac)_2$ and NaOH was employed to make a ZnO coating on the $CaCu_3Ti_4O_{12}$ nanoparticles.[18–21] In this work, 1.468 g (0.008 mol) $Zn(Ac)_2$ and 1.228 g $CaCu_3Ti_4O_{12}$ nanoparticles were dissolved in 800 mL of deionized water with constant stirring for 30 min at 800 rpm. Then 800 mL of 0.1 M NaOH aqueous solution was added dropwise and the resulting solution was kept stirring for 5 hours to get a good dispersion. To form ZnO grains on the surface of the dispersed $CaCu_3Ti_4O_{12}$ nanoparticles, the solution was finally refluxed at 100 °C for 5 hours. After cooling down to room temperature, the product was filtered with a 0.22 μm membrane and washed with deionized water twice and then vacuum dried to afford core-satellite $CaCu_3Ti_4O_{12}$@ZnO nanofillers.

2.3 Preparation of silicone rubber composites

Fillers ($CaCu_3Ti_4O_{12}$, ZnO and $CaCu_3Ti_4O_{12}$@ZnO) should be processed by silane coupling agent KH-151 to get a better dispersion in the silicone rubber. 110 methyl vinyl silicone rubber and vulcanizing agent were mixed in an open mill for 30 min. According to the composition of insulated silicone rubber, 5 wt% muscovite was added into the rubber for easy demould; meanwhile 50 wt% fumed silica and 30 wt% aluminium hydroxide were added for strength and flame retardancy. Then the pre-processed fillers were evenly added into the silicone rubber and milled for 2 hours. The filler mass fraction ranged from 20 wt% to 60 wt% as shown in Table 1. Finally, the composites were pressed with a vulcanizing machine in the mould at 15 MPa and 175 °C for 10 min, and then cooled down to room temperature. The fillers ($CaCu_3Ti_4O_{12}$, ZnO and $CaCu_3Ti_4O_{12}$@ZnO)-doped silicone rubber composite samples were about 200 μm in thickness and 30 mm in diameter.

2.4 Characterization

X-ray diffraction (XRD) measurements were carried out using a X-ray diffractometer (Rigaku, D/max 2500 PC) with Cu K_α radiation (λ = 1.5406 Å). 40 kV and 200 mA were applied. The continuous scan speed was 5° min^{-1}. The morphology of the

Table 1 Samples prepared with different fillers added ranging from 20 to 60 wt%

Designation	ZnO	$CaCu_3Ti_4O_{12}$	$CaCu_3Ti_4O_{12}$@ZnO
N	—	—	—
20Z	20.0	—	—
30Z	30.0	—	—
40Z	40.0	—	—
50Z	50.0	—	—
20C	—	20.0	—
30C	—	30.0	—
40C	—	40.0	—
50C	—	50.0	—
20M	6.7	13.3	—
30M	10.0	20.0	—
40M	13.3	27.7	—
50M	16.7	33.3	—
60M	20.0	40.0	—
20CS	—	—	20.0
30CS	—	—	30.0
40CS	—	—	40.0
50CS	—	—	50.0
60CS	—	—	60.0

fillers was examined by field emission scanning electron microscopy (SEM, ZEISS SUPRA^R 55) and field emission transmission electron microscopy (TEM, FEI Tecnai G^2 F30, 300 kV). The elemental analysis of $CaCu_3Ti_4O_{12}$@ZnO fillers was carried out by energy dispersive X-ray spectrometry (EDS, Oxford X-Max 20). The thermal stability of the composites was examined by thermogravimetric analysis (TGA, Mettler-Toledo TGA/DSC 1, STAR^e System) with a heating rate of 10 °C min^{-1} from 50 to 800 °C under nitrogen flow (50 mL min^{-1}). The surface analysis of the fillers and samples was performed by X-ray photoelectron spectrometry (XPS, ESCALAB 250Xi, Thermo Fisher, UK) using Ar ion beam etching for 50 s, which could show the bonding details. Focused monochromatized Al Kα radiation at a pass energy of 20 eV was applied. The energy scale was calibrated and corrected using the C 1s (284.6 eV) line as the binding energy reference. The nonlinear electrical characteristics of composites were analyzed by the low frequency module (Alpha-A High Performance Frequency Analyzer) of a broadband dielectric analyzer (Concept 80, Novocontrol GmbH, Germany), and samples were sandwiched between two 20 mm gold plated electrodes tested with active sample cell. With a frequency of 50 Hz, the test voltage ranged from 0 V to 1400 V. All the measurements were obtained at room temperature.

3. Results and discussion

3.1 XRD measurements

The diffraction patterns of ZnO, $CaCu_3Ti_4O_{12}$ and $CaCu_3Ti_4$-O_{12}@ZnO nanoparticles are shown in Fig. 1(a). The peak positions of the XRD patterns fitted well with reported values of ZnO phase (JCPDS PDF#80-0074) and $CaCu_3Ti_4O_{12}$ phase (JCPDS PDF#75-2188), which indicated that ZnO here was wurtzite and $CaCu_3Ti_4O_{12}$ perovskite-like. The XRD results revealed that the "core" and "satellite" of the synthesized core-satellite

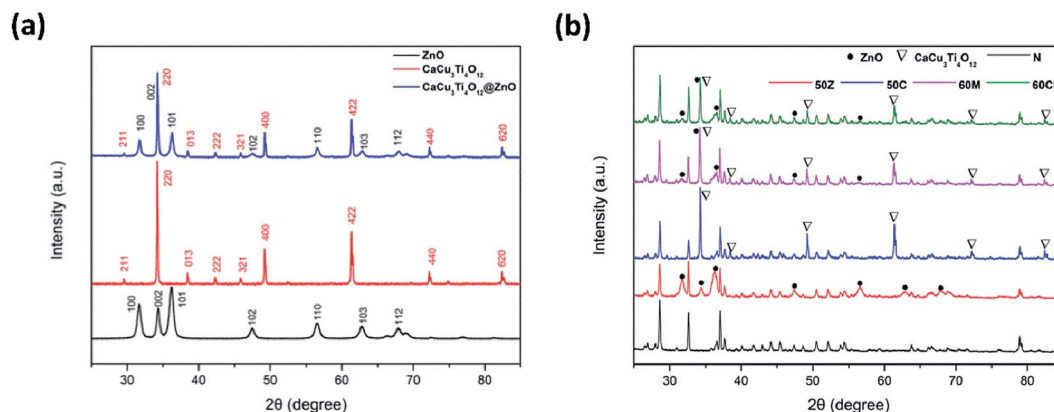**Fig. 1** XRD patterns of fillers and samples. (a) ZnO, $CaCu_3Ti_4O_{12}$ and $CaCu_3Ti_4O_{12}$@ZnO nanoparticles. (b) N, 50Z, 50C, 60M and 60CS samples.

$CaCu_3Ti_4O_{12}$@ZnO nanoparticles had the same crystal structure as $CaCu_3Ti_4O_{12}$ and ZnO fillers respectively. The diffraction patterns of N, 50Z, 50C, 60M and 60CS samples are shown in Fig. 1(b). Compared with N sample, 50Z displayed the peak positions of ZnO phase, and 50C displayed those of $CaCu_3Ti_4O_{12}$ phase. Meanwhile, 60M and 60CS showed the same peak positions of ZnO phase and $CaCu_3Ti_4O_{12}$ phase. It is confirmed that the ZnO and $CaCu_3Ti_4O_{12}$ doped silicone rubber composites could be the reference groups of the $CaCu_3Ti_4O_{12}$@ZnO doped silicone rubber composites which were the focus of this work.

3.2 Electron microscopy and EDS analysis

Fig. 2(a–c) shows SEM micrographs of ZnO, $CaCu_3Ti_4O_{12}$ and core-satellite $CaCu_3Ti_4O_{12}$@ZnO fillers respectively. The ZnO grains possessed typical features of wurtzite structure. The average grain size was about 50 nm. The $CaCu_3Ti_4O_{12}$ grains were tetragonal perovskite-like, and the average grain size was

about 500 nm. As can be seen from Fig. 2(c), perovskite-like $CaCu_3Ti_4O_{12}$ particles were surrounded by large numbers of ZnO nanoparticles, and the average particle size of ZnO was also about 50 nm. Either the crystalline phase or the particle size was the same as the pure phase ZnO and $CaCu_3Ti_4O_{12}$ particles. Fig. 2(d) shows a TEM micrograph of the core-satellite $CaCu_3Ti_4O_{12}$@ZnO particles. The ZnO nanoparticles adsorbed onto the surface of the bigger $CaCu_3Ti_4O_{12}$ particles, which was consistent with the SEM result. Because of the high surface energy of nanoparticles, agglomeration occurred easily, which indicated that the pre-processing of the fillers was an important procedure to get better dispersion in the silicone rubber composites.

The EDS analysis of the core-satellite $CaCu_3Ti_4O_{12}$@ZnO is shown in Fig. 3. The atomic ratio was found to be Zn : Cu : Ca : Ti = 12.5 : 10.3 : 3.4 : 13.9. The mass ratio between $CaCu_3Ti_4O_{12}$ core and ZnO satellite could be calculated to be 2 : 1. This was why the mass ratio between $CaCu_3Ti_4O_{12}$
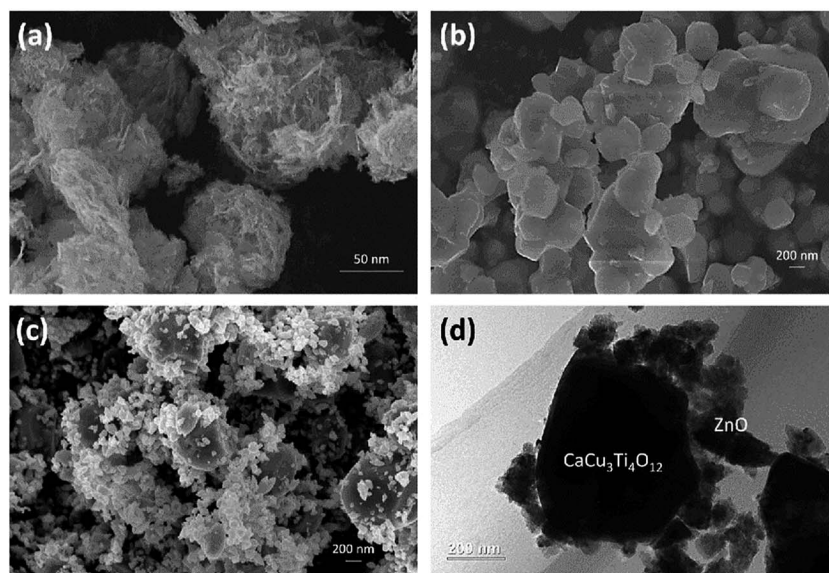

Fig. 2 SEM micrographs of (a) ZnO, (b) $CaCu_3Ti_4O_{12}$ and (c) core-satellite $CaCu_3Ti_4O_{12}$@ZnO fillers. (d) TEM micrograph of a core-satellite $CaCu_3Ti_4O_{12}$@ZnO particle.

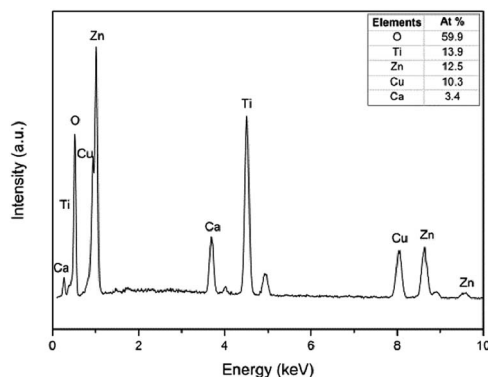**Fig. 3** EDS analysis of the core-satellite $CaCu_3Ti_4O_{12}$@ZnO. The inset table shows the atomic ratios.
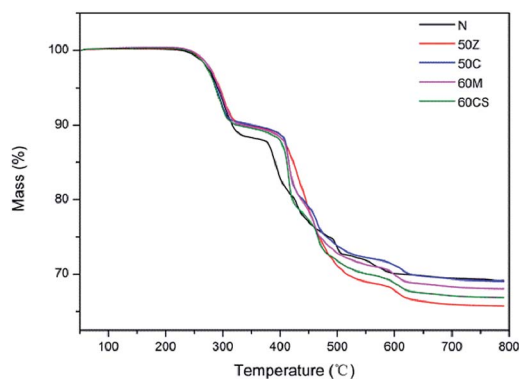

Fig. 4 TGA curves of N, 50Z, 50C, 60M and 60CS samples.

and ZnO fillers in 20M, 30M, 40M and 50M was 2 : 1, which were prepared to be the reference groups.

3.3 Thermal behavior of the composites

The thermal behavior of the silicone rubber composites at a constant heating rate of 10 °C min^{-1} was investigated. The TGA curves of N, 50Z, 50C, 60M and 60CS samples are given in Fig. 4. There was almost no weight loss below 250 °C, which

indicated that the silicone rubber composites had good thermal stability in this temperature range. When the temperature was higher than 250 °C, there were two typical weight loss stages.[22] The first stage appeared at about 250 to 300 °C with a weight loss of about 10%, which was attributed to the decomposition of aluminium hydroxide $(Al(OH)_3)$ in the composites. The second weight loss stage appeared at about 400 to 600 °C. In this stage, the polysiloxane chains began to break, such as the chemical bonds Si–O and Si–C, which resulted in a weight loss of about 20%. Therefore when the application temperature was lower than 250 °C, the composites exhibited excellent thermal stability.

3.4 XPS analysis

XPS was used to characterize the bonding of core-satellite $CaCu_3Ti_4O_{12}$@ZnO fillers. Since $CaCu_3Ti_4O_{12}$ particles were surrounded by small ZnO grains on the outside, Zn 2p was chosen to be the detected species. Fig. 5(a) shows the XPS analysis of the fillers. The Zn 2p peaks of "$CaCu_3Ti_4O_{12}$ + ZnO" fillers are located at 1021.99 eV and 1044.99 eV, and those of $CaCu_3Ti_4O_{12}$@ZnO fillers at 1021.80 eV and 1044.80 eV. With the peak shift of 0.19 eV, the binding energy of Zn 2p in $CaCu_3Ti_4O_{12}$@ZnO decreased, which indicated that there was chemical bonding between the $CaCu_3Ti_4O_{12}$ core and ZnO satellites. Fig. 5(b) shows the XPS analysis of 60M and 60CS samples which were doped with "$CaCu_3Ti_4O_{12}$ + ZnO" and $CaCu_3Ti_4O_{12}$@ZnO fillers respectively. The Zn 2p peaks of 60M samples presented at 1022.68 eV and 1045.68 eV, and those of 60CS presented at 1022.52 eV and 1045.52 eV. The peak shift was 0.16 eV. It is confirmed that there was still bonding between $CaCu_3Ti_4O_{12}$ and ZnO grains after $CaCu_3Ti_4O_{12}$@ZnO fillers were doped into the silicone rubber. The XRD pattern of 60M had shown the presence of $CaCu_3Ti_4O_{12}$ and ZnO phases, which showed that $CaCu_3Ti_4O_{12}$@ZnO fillers still retained the core-satellite structure in the matrix.

3.5 Nonlinear conductive characteristics

The J–E characteristics of ZnO/silicone rubber composites with filler content from 20 wt% to 50 wt% are shown in Fig. 6(a). A
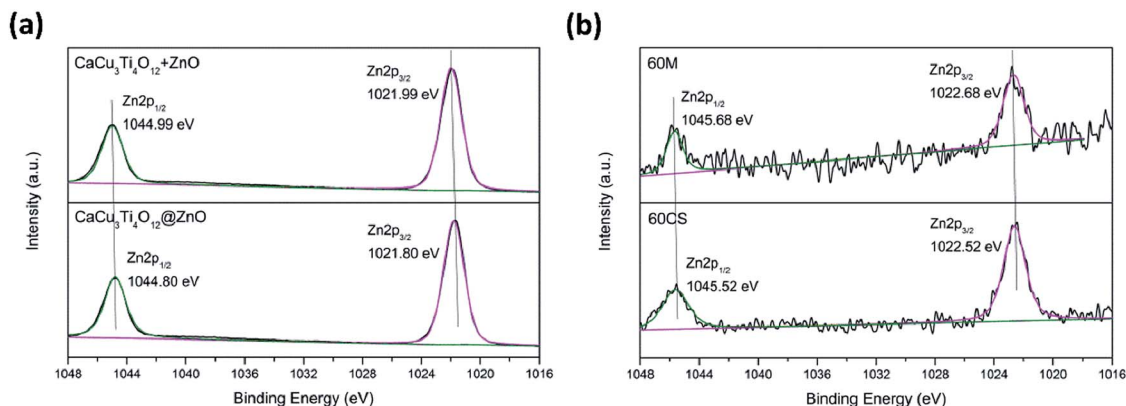

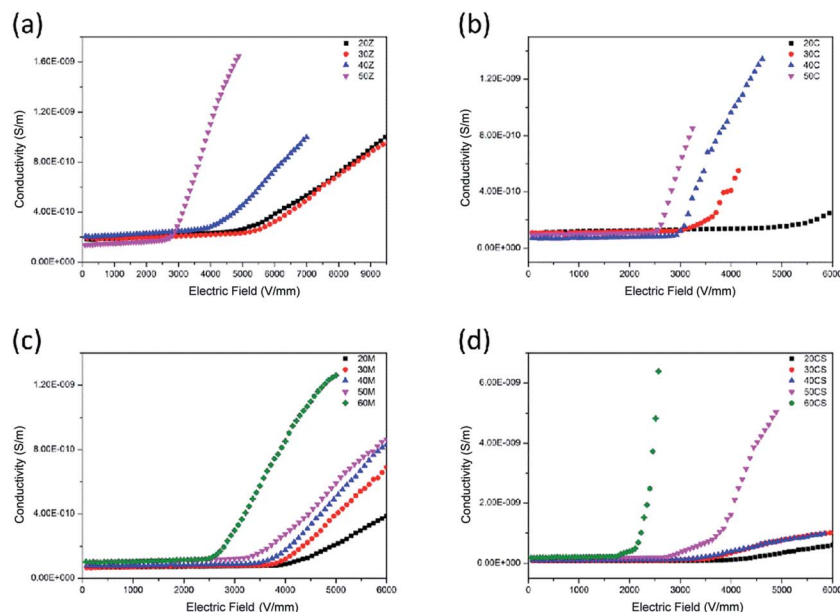**Fig. 5** XPS (Zn 2p) analysis of fillers and samples. (a) $CaCu_3Ti_4O_{12}$ + ZnO and $CaCu_3Ti_4O_{12}$@ZnO; (b) 6OM and 60CS samples.

Fig. 6 The J–E characteristics of silicone rubber composites doped with (a) ZnO, (b) $CaCu_3Ti_4O_{12}$, (c) mixture of $CaCu_3Ti_4O_{12}$ and ZnO and (d) core-satellite $CaCu_3Ti_4O_{12}$@ZnO fillers.

typical way to evaluate the nonlinear conductive properties of the composites is to compare the nonlinear conductive coefficient α_j,[10,23] which can be calculated by eqn (1):

$$\alpha_j = \frac{\log(J_2/J_1)}{\log(E_2/E_1)} \tag{1}$$

where $J_2 = 1 \times 10^{-9}$ S m^{-1}, $J_1 = 3 \times 10^{-10}$ S m^{-1}, E_2 and E_1 are the corresponding electric field of J_1 and J_2 according to the measured J–E curve. E_1 is defined as the switching field E_b. Results indicated that samples with filler content from 20 wt% to 50 wt% exhibited stable nonlinear conductive behaviors, and the composites showed α_j of 2.18, 2.30, 2.32 and 4.61 respectively. With filler concentration increasing, the nonlinear conductive coefficient α_j became larger, and the switching field decreased. Fig. 6(b) shows the J–E characteristics of $CaCu_3Ti_4O_{12}$/silicone rubber composites with filler content from 20 wt% to 50 wt%. The nonlinear conductive coefficient α_j was 2.81, 5.33, 8.08, 9.33, respectively. They had the same trends as the

ZnO/silicone rubber composites. It was shown that SiC/silicone rubber composites exhibited an α_j of 4.1,[24] which was slightly larger than that of ZnO/silicone rubber composites, but smaller than that of $CaCu_3Ti_4O_{12}$/silicone rubber composites. This indicated that ZnO and $CaCu_3Ti_4O_{12}$ nanoparticles were promising fillers to tailor the nonlinear conductive properties.

Percolation theory is often introduced in the process of explaining the conduction mechanism of conductive composites.[25,26] As shown in Fig. 7(a and b), when the filler concentration is higher than the percolation threshold, particles in the matrix would contact, which would form current paths. For ZnO or $CaCu_3Ti_4O_{12}$ n-type semiconducting grains, Schottky barriers were created at the interfaces in many cases.[27] Therefore, J–E would follow the relationship of eqn (2):[28–33]

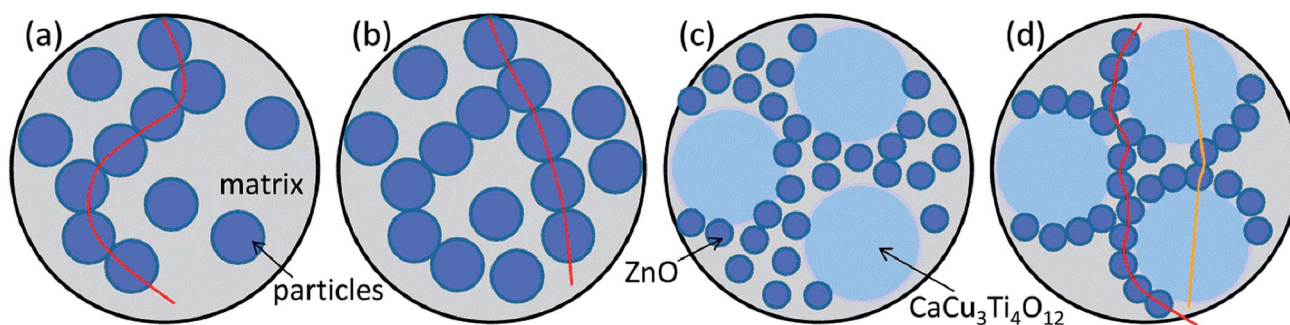$$J = AT^2 \exp\left[\frac{\beta\sqrt{V} - V_B}{k_B T}\right] \tag{2}$$

Fig. 7 A schematic diagram of filler distribution and possible current paths. (a) Filler concentration higher than percolation threshold; (b) relatively higher filler concentration; (c) mixture of $CaCu_3Ti_4O_{12}$ and ZnO; (d) core-satellite $CaCu_3Ti_4O_{12}$@ZnO. The red and orange lines represent possible current paths.

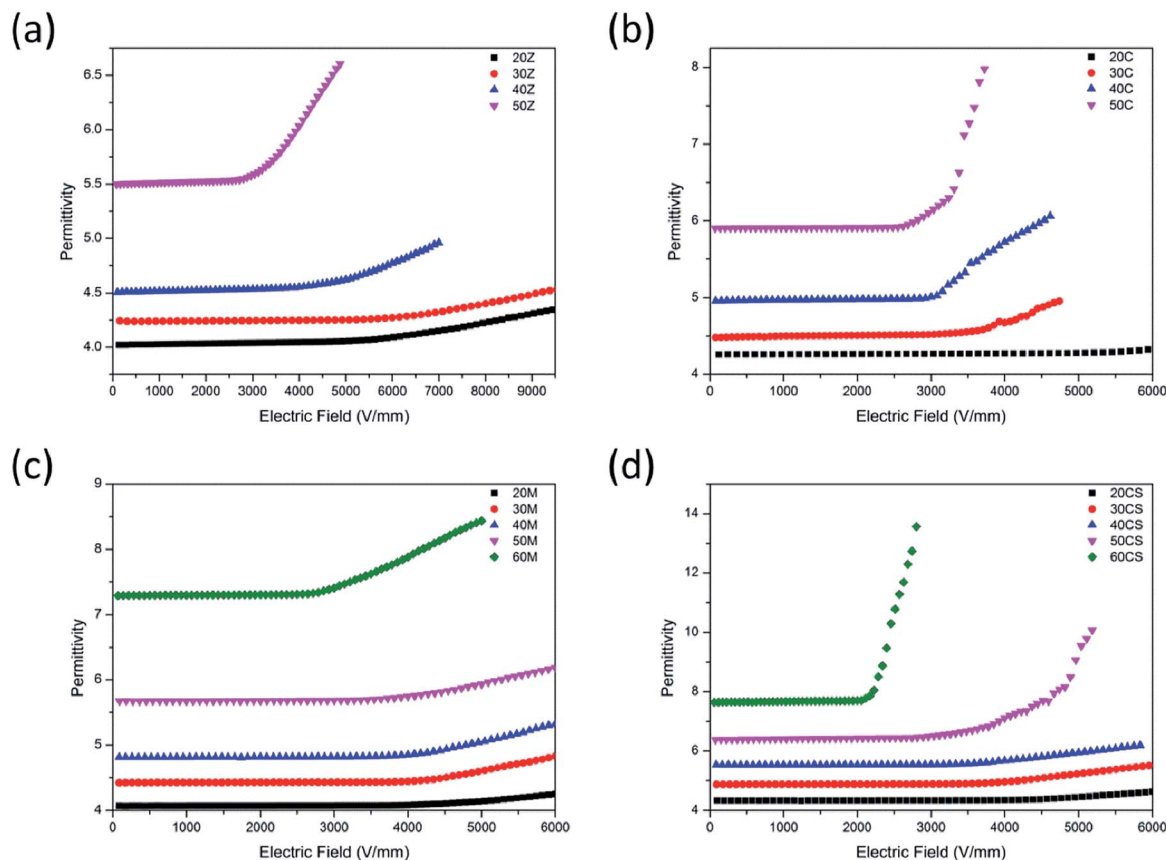**Fig. 8** The ε–E characteristics of silicone rubber composites doped with (a) ZnO, (b) CaCu$_3$Ti$_4$O$_{12}$, (c) mixture of CaCu$_3$Ti$_4$O$_{12}$ and ZnO and (d) core-satellite CaCu$_3$Ti$_4$O$_{12}$@ZnO fillers.

where A is the Richardson constant, k_B the Boltzmann constant, V_B the barrier height, and β a constant related to barrier width. The composites therefore exhibit nonlinear conductive properties with temperature constant.

If the concentration of fillers is relatively high, more current paths would come into being. The current may transport *via* the shortest path, which leads to lower switching field and larger nonlinear conductive coefficient. It has been reported that CaCu$_3$Ti$_4$O$_{12}$ has remarkably strong nonlinear characteristics and the nonlinear coefficient of CaCu$_3$Ti$_4$O$_{12}$ is even greater than that of ZnO.[14] The nonlinear conductive properties of both ZnO and CaCu$_3$Ti$_4$O$_{12}$ nanoparticle-doped silicone rubber composites could be explained by this schematic diagram.

Fig. 6(c) shows the J–E characteristics of composites doped by a mixture of CaCu$_3$Ti$_4$O$_{12}$ and ZnO (mass ratio = 2 : 1) from 20 wt% to 60 wt%. The nonlinear conductive coefficient α_j was 2.72, 3.25, 3.62, 4.03, 4.31, respectively. Fig. 6(d) shows the J–E characteristics of CaCu$_3$Ti$_4$O$_{12}$@ZnO/silicone rubber composites with filler content from 20 wt% to 60 wt%. The nonlinear conductive coefficient α_j was 3.46, 3.95, 4.00, 6.91, 10.87, respectively, which was larger than that of mixed particle-doped silicone rubber composites. The mixture of ZnO and CaCu$_3$Ti$_4$O$_{12}$ particles were dispersed in the matrix (Fig. 7(c)), so that it was very hard to form a current path unless the concentration of fillers was high enough. The particle size of the core-satellite

CaCu$_3$Ti$_4$O$_{12}$@ZnO was larger than either ZnO or CaCu$_3$Ti$_4$-O$_{12}$, for which the particles contacted easily. The ZnO nanoparticles adsorbed onto the surface of CaCu$_3$Ti$_4$O$_{12}$ could form a 3D structure for the current paths. And even ZnO–CaCu$_3$Ti$_4$-O$_{12}$ contact could form a path too (Fig. 7(d)). The current transport could choose more and shorter paths, leading to lower switching field and larger nonlinear conductive coefficient.

3.6 Nonlinear dielectric characteristics

Similar to the nonlinear conductive coefficient, the nonlinear dielectric coefficient α_ε of composites can be calculated by eqn (3):[10]

$$\alpha_\varepsilon = \frac{\log(\varepsilon_2/\varepsilon_1)}{\log(E_2/E_1)} \tag{3}$$

where E_1 is the switching field E_b, ε_1 and ε_2 are the corresponding permittivity of E_1 and E_2 according to the measured ε–E curve.

The ε–E characteristics of ZnO/silicone rubber composites with filler content from 20 wt% to 50 wt% are shown in Fig. 8(a). As can be seen, the permittivity of the composites increased with filler concentration. Within low electric field, the permittivity of ZnO/silicone rubber composite with 50 wt% filler content reached 5.5. The nonlinear dielectric coefficient α_ε of
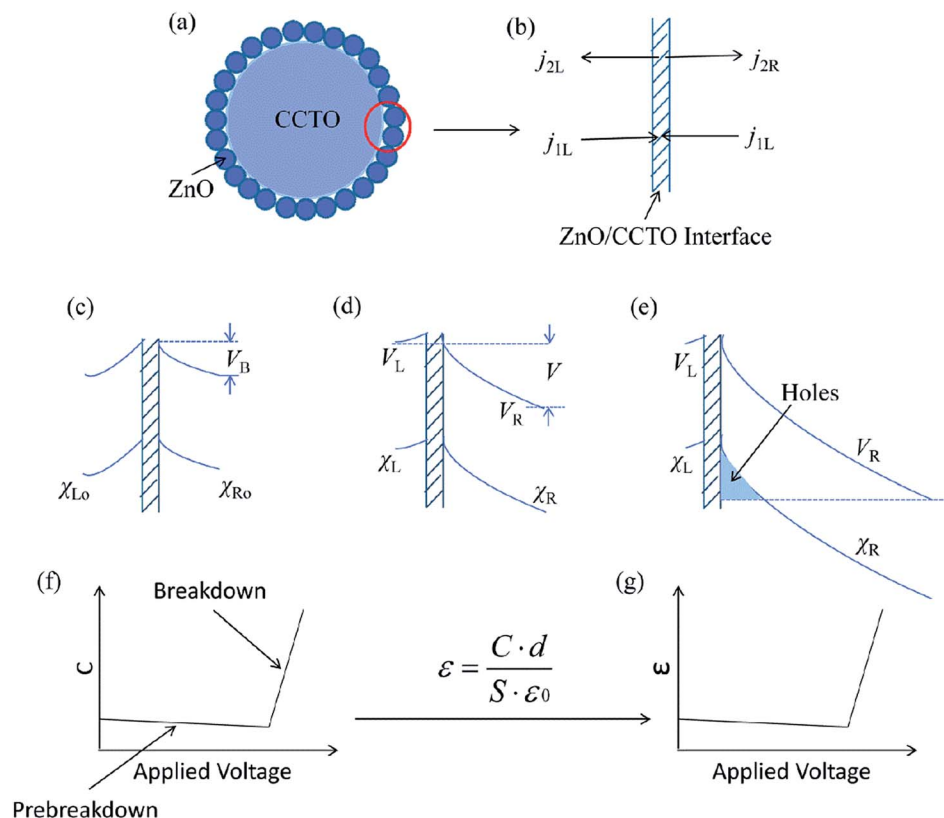
Fig. 9 (a) A core-satellite CaCu$_3$Ti$_4$O$_{12}$ particle. (b) Two-step model in the prebreakdown region. (c) Double-depletion-layer model at zero applied voltage. (d) The application of V causes V_R to increase and V_L to decrease. (e) The hole model in the breakdown region. (f) Capacitance *versus* applied junction voltage. (g) Permittivity *versus* applied junction voltage.

ZnO/silicone rubber composites also got larger with filler concentration. The ZnO/silicone rubber composite with 50 wt% filler content exhibited an α_ε of 0.35. Fig. 8(b) shows the ε–E characteristics of CaCu$_3$Ti$_4$O$_{12}$/silicone rubber composites with filler content from 20 wt% to 50 wt%. The permittivity of the composites increased with filler concentration too. With the same filler concentration, the permittivity of CaCu$_3$Ti$_4$-O$_{12}$/silicone rubber composites was slightly larger than that of ZnO/silicone rubber composites, since the permittivity of CaCu$_3$Ti$_4$O$_{12}$ particles was larger than that of ZnO particles. Composites with 20 wt% CaCu$_3$Ti$_4$O$_{12}$ fillers failed to exhibit stable nonlinear dielectric behaviors. With larger filler concentration, the composites showed an α_ε of 0.29, 0.44 and 1.02 with 30 wt%, 40 wt% and 50 wt% filler concentration, respectively. Fig. 8(c) shows the ε–E characteristics of composites doped with a mixture of CaCu$_3$Ti$_4$O$_{12}$ and ZnO (mass ratio = 2 : 1) from 20 wt% to 60 wt%. It is obvious that the composites showed little nonlinearity. The largest nonlinear dielectric coefficient α_ε was 0.26. Fig. 8(c) is in sharp contrast to Fig. 8(d) which shows the ε–E characteristics of CaCu$_3$Ti$_4$O$_{12}$@ZnO/silicone rubber composites with filler content from 20 wt% to 60 wt%. The composites showed stable nonlinear dielectric properties with 50% wt% and 60 wt% filler concentration whose α_ε was 1.30 and 2.33, respectively. Comparing Fig. 8(a–d), the composites doped with a mixture of CaCu$_3$Ti$_4$O$_{12}$ and ZnO showed worse nonlinearity than either ZnO or CaCu$_3$Ti$_4$O$_{12}$ doped composites.

However, the CaCu$_3$Ti$_4$O$_{12}$@ZnO/silicone rubber composites showed not only the highest permittivity within low electric field but also the best nonlinearity. It is evident that the core-satellite structure played the key role in the nonlinear dielectric properties of the composites.

Fig. 9(a) shows the structure of a core-satellite CaCu$_3$Ti$_4$-O$_{12}$@ZnO particle. XPS analysis had indicated that there was bonding between core and satellite, so the interfaces could serve as internal capacitors between ZnO and CaCu$_3$Ti$_4$O$_{12}$ grains.[10,12,13,34] The double-depletion-layer model is introduced at first, which appears to be generally accepted. Fig. 9(c) shows the double-depletion-layer model at zero applied voltage. There was a depletion region in both ZnO semiconductor side and CaCu$_3$Ti$_4$O$_{12}$ semiconductor side,[14] of width χ_{Lo} and χ_{Ro} on the left and right side. And the barrier height was V_B. Fig. 9(d) shows the application of a positive voltage V on the region. On the right side, the conduction band was lowered and the depletion region was widened, so that V_R and χ_R increased. To explain the nonlinearity of the composites, we separated it into two parts, the prebreakdown region and breakdown region, which were in the low voltage region and the high voltage region, respectively.

In the prebreakdown region, the two-step model was introduced for charge transport.[34] It was assumed that an electron transferred from the grain to the interface, and then on to the other grain, which were separate steps in charge transport. The four transport current flows are defined in Fig. 9(b). The

junction capacitance C in this model could be calculated by eqn (4):[34]

$$C = \frac{\mathrm{d}Q}{\mathrm{d}V} \approx \frac{C_0}{\sqrt{(1 + V/V_B)}} \qquad (4)$$

where C_0 is the capacitance at zero applied voltage. C decreases slowly with V. Therefore the capacitance showed a slow decrease with increasing applied voltage in the prebreakdown region.

In the breakdown region, when the applied voltage increased much above the breakdown voltage, the conduction band would drop below the top of the valance band on the same side of the junction. Holes came into being, causing thinning of the potential barrier to electrons tunneling from the interface, as can be seen in Fig. 9(e). By evaluating the total energy ξ and its second derivative with respect to V, the capacitance could be calculated by eqn (5) and (6):[34]

$$\xi = \frac{\varepsilon_0 A}{8\pi} \int \mathrm{d}x \left(\frac{\mathrm{d}U}{\mathrm{d}x}\right)^2 \qquad (5)$$

$$C = \frac{d^2}{\mathrm{d}V^2}\xi \qquad (6)$$

In the breakdown region, the calculated result is shown in Fig. 9(f) in which the capacitance then rises quite steeply. In other words, with holes coming into being, the charge became large, but the distance between the holes and the electrons in the interface was smaller, which resulted in the steep rise of the capacitance.

Combining the prebreakdown region and the breakdown region, the capacitance exhibited nonlinearity with applied voltage. The permittivity was positive relative to the capacitance, which was expressed by eqn (7):

$$\varepsilon = \frac{Cd}{S\varepsilon_0} \qquad (7)$$

where d is the distance between the electrodes, S the area of the capacitor, and ε_0 the vacuum permittivity. Thus the permittivity showed obvious nonlinearity and the composites exhibited nonlinear dielectric properties, which is shown in Fig. 9(g).

4. Conclusions

By doping the synthesized core-satellite CaCu$_3$Ti$_4$O$_{12}$@ZnO into silicone rubber, composites with both nonlinear conductive and nonlinear dielectric characteristics were fabricated using nanoparticle fillers for the first time. The XPS and XRD results showed that there was bonding between ZnO and CaCu$_3$Ti$_4$O$_{12}$, which restrained the core-satellite structure tightly. The nonlinear conductive coefficient α_j of CaCu$_3$Ti$_4$O$_{12}$@ZnO/silicone rubber composites with a filler concentration 60 wt% was 10.87, and the nonlinear dielectric coefficient α_ε was 2.33. Both the nonlinear conductive coefficient and dielectric coefficient increased with filler concentration. The classical current-path model was utilized to explain the nonlinear conductive properties, while the interface-barrier-layer-capacitor model and double-depletion-layer model were introduced to explain the nonlinear dielectric properties, which would broaden the thinking for the fabrication of nonlinear composites.

References

1 T. Christen, L. Donzel and F. Greuter, *IEEE Electr. Insul. Mag.*, 2010, **6**, 47–59.

2 L. Donzel, F. Greuter and T. Christen, *IEEE Electr. Insul. Mag.*, 2011, **2**, 18–29.

3 J. Robertson and B. R. Varlow, *Properties and Applications of Dielectric Materials, Proceedings of the 7th International Conference on IEEE*, 2003, vol. 2, pp. 761–764.

4 B. R. Varlow and K. Li, *IEE Proc.-A: Sci., Meas. Technol.*, 2003, **150**, 75–82.

5 E. A. Cherney, *IEEE Electr. Insul. Mag.*, 2013, **29**, 59–65.

6 M. Paredes-Olguin, C. Gomez-Yañez, F. P. Espino-Cortes and E. Ramirez, *IEEE Trans. Dielectr. Electr. Insul.*, 2013, **20**, 2335–2342.

7 J. Glenneberg, M. Zenkner, G. Wagner, S. Lemm, C. Ehrhardt, W. Münchgesang, A. Buchsteiner, M. Diestelhorst, H. Beige and S. Ebbinghaus, *RSC Adv.*, 2014, **4**, 61268–61276.

8 K. Eda, *IEEE Electr. Insul. Mag.*, 1989, **5**, 28–30.

9 T. K. Gupta, *J. Am. Ceram. Soc.*, 1990, **73**, 1817–1840.

10 L. Gao, X. Yang, J. Hu and J. He, *Mater. Lett.*, 2016, **171**, 1–4.

11 M. Subramanian, D. Li, N. Duan, B. Reisner and A. Sleight, *J. Solid State Chem.*, 2000, **151**, 323–325.

12 R. Schmidt, S. Pandey, P. Fiorenza and D. C. Sinclair, *RSC Adv.*, 2013, **3**, 14580–14589.

13 L. Sun, R. Zhang, Z. Wang, E. Cao, Y. Zhang and L. Ju, *RSC Adv.*, 2016, **6**, 55984–55989.

14 S.-Y. Chung, I.-D. Kim and S.-J. L. Kang, *Nat. Mater.*, 2004, **3**, 774–778.

15 D. R. Clarke, *J. Am. Ceram. Soc.*, 1999, **82**, 485–502.

16 T. Tanaka, *IEEE Trans. Dielectr. Electr. Insul.*, 2005, **12**, 914–928.

17 T. Tanaka, M. Kozako, N. Fuse and Y. Ohki, *IEEE Trans. Dielectr. Electr. Insul.*, 2005, **12**, 669–681.

18 X. L. Zhang, Y. H. Kim and Y. S. Kang, *Solid State Phenomena*, Trans Tech Publications, 2007, vol. 119, pp. 239–242.

19 S. Kanmani and K. Ramachandran, *Renewable Energy*, 2012, **43**, 149–156.

20 D. Zhu, W. Li, L. Ma and Y. Lei, *RSC Adv.*, 2014, **4**, 9372–9378.

21 Z. Wang, L. Wu, J. Zhou, B. Shen and Z. Jiang, *RSC Adv.*, 2013, **3**, 3309–3315.

22 S. Béfahy, P. Lipnik, T. Pardoen, C. Nascimento, B. Patris, P. Bertrand and S. Yunus, *Langmuir*, 2009, **26**, 3372–3375.

23 X. Yang, J. He and J. Hu, *J. Appl. Polym. Sci.*, 2015, **132**, 40.

24 F. Wang, P. Zhang, M. Gao, X. Zhao and J. Gao, *Electrical Insulation and Dielectric Phenomena (CEIDP), IEEE Conference on IEEE*, 2013, pp. 435–538.

25 Y. Jiangao, L. Chengcen and S. Kai, *Res. Chem. Intermed.*, 2006, **2**, 13–17.

26 I. Balberg, D. Azulay, D. Toker and O. Millo, *Int. J. Mod. Phys. B*, 2004, **18**, 2091–2121.

27 D. Capsoni, M. Bini, V. Massarotti, G. Chiodelli, M. C. Mozzatic and C. B. Azzoni, *J. Solid State Chem.*, 2004, **177**, 4494–4500.

28 K. Eda, *J. Appl. Phys.*, 1978, **49**, 2964–2972.

29 S. A. Pianaro, P. R. Bueno, P. Olivi, E. Longo and J. A. Varela, *J. Mater. Sci. Lett.*, 1997, **16**, 634–638.

30 G. Zang, J. Zhang, P. Zheng, J. Wang and C. Wang, *J. Phys. D: Appl. Phys.*, 2005, **38**, 1824.

31 J. Y. Wang, F. J. Wang, P. C. Li, C. H. Chen, B. W. Su and L. W. Zhong, *Eur. Phys. J.: Appl. Phys.*, 2000, **11**, 155–158.

32 L. Liu, L. Fang, Y. Huang and Y. Li, *J. Appl. Phys.*, 2011, **110**, 094101–094106.

33 L. Liu, Y. Huang, Y. Li, D. Shi, S. Zheng, S. Wu, L. Fang and C. Hu, *J. Mater. Sci.*, 2012, **47**, 2294–2299.

34 G. Mahan, L. M. Levinson and H. R. Philipp, *J. Appl. Phys.*, 1979, **50**, 2799–2812.